Journal of Crystal Growth 603 (2023) 127024

Contents lists available at ScienceDirect

Journal of Crystal Growth

journal homepage: www.elsevier.com/locate/jcrysgro

Cluster-mediated stop-and-go crystallization

A.E.S. Van Driessche [a,*], J. Lutsko [b], D. Maes [c], M. Sleutel [c,d,*]

[a] Instituto Andaluz de Ciencias de la Tierra, IACT, CSIC – University of Granada, Avenida de las Palmeras 4, 18100, Armilla (Granada), Spain.
[b] Center for Nonlinear Phenomena and Complex Systems, Code Postal 231, Université Libre de Bruxelles, Boulevard du Triomphe, 1050 Brussels, Belgium
[c] Structural Biology Brussels, Vrije Universiteit Brussel, Pleinlaan 2, 1050 Brussels, Belgium
[d] Structural and Molecular Microbiology, VIB-VUB Center for Structural Biology, VIB, Pleinlaan 2, 1050 Brussels, Belgium

ARTICLE INFO

Communicated by: J. De Yoreo

Keywords:
A1 cluster-mediated growth
A1 impurities
A1 in situ observation step dynamics
A1 kinetic monte carlo
A1 dead zone
A1 biocrystallization

ABSTRACT

Impurities control the formation of bio-crystals and can fully paralyze crystal growth at low levels of supersaturation. Traditional impurity models predict that an escape from this so-called "dead zone" requires an increase in the driving force (i.e. supersaturation). In this work, using protein crystals as a model system, we uncover an alternative escape route from the dead zone that does not involve an increase in supersaturation. We demonstrate that the merger of a protein cluster with the crystal surface triggers the formation of an ordered multi-layered island. The newly created surface on top of the resulting 3D island is initially devoid of impurities and therefore characterized by near-pure step growth kinetics. The accelerated step advancement on this relatively uncontaminated surface limits the available time for impurities to adsorb on the emerging terraces and by extension their resulting surface density. Cluster-mediated crystal growth occurring in heterogeneous media can therefore lead to stop-and-go dynamics, which offers a new model to explain crystallization taking place under biological control (e.g. biomineralization).

1. Introduction

The presence of solute species that are distinct from the crystal-building units is an unavoidable reality in any instance of crystal growth, even under highly controlled laboratory settings. These foreign molecules (i.e. impurities/additives) interact differently with the lattice in comparison to the main building blocks due to their physico-chemical differences. Through their interaction with the crystal surface they can modulate the crystal's surface growth energetics and/or kinetics [1]. Identifying the nature and the role of impurity effects is a key step in understanding biomineralization, controlling the industrial crystallization process of e.g. pharmaceutical compounds and preventing scale formation using additives [2]. The foundations of crystal growth kinetics require a fundamental understanding of the processes that determine the flux of growth units from the mother liquor to the step edges. It is perhaps difficult to overstate the contributions of A.A. Chernov to this field of crystallization, be it under pure or impure conditions. The authors A.E.S. Van Driessche and M. Sleutel recall that Chernov's book *Modern Crystallography 3* served as a tremendous source of information and inspiration during their formative years. The authors are convinced that this classic textbook has been a companion to many burgeoning scientists that are pursuing crystal growth topics.

While most studies focus on the mechanisms of additive-induced growth retardation/inhibition and the morphological outcome, less attention has been paid to the recovery of surfaces from impurity poisoning. Nonetheless, this is a key component in biomineralization where pulsed growth is often observed. Similarly, formation of scale deposits can also be viewed as a stop-and-go crystallization process that follows from the oscillations in the solute composition. As a general rule of thumb, arrested surfaces will overcome the impurity blockade when the driving force for crystallization is increased. In most formal treatments, only elementary steps are considered e.g. [3,4]. But, experiments have shown for the case of potassium dihydrogen phosphate that macrosteps (bunches of monolayer steps) can propel the surface out of the dead zone [5] (i.e. supersaturated region were step movement is fully blocked due to the impurity action). Although this mechanism of growth recovery was initially not well understood, we recently proposed a model for macrostep-mediated impurity recovery based on kinetic Monte Carlo simulations[6]. Related to this are our observations for protein crystal growth, which revealed that protein clusters can also accelerate the recovery of an impurity-poisoned surface by merging with the latter [7]. This observation becomes especially relevant considering

* Corresponding authors at: Instituto Andaluz de Ciencias de la Tierra, IACT, CSIC – University of Granada, Avenida de las Palmeras 4, 18100, Armilla (Granada), Spain. (A.E.S. Van Driessche) and Structural Biology Brussels, Vrije Universiteit Brussel, Pleinlaan 2, 1050, Brussels, Belgium (M. Sleutel)
E-mail addresses: alexander.vd@csic.es (A.E.S. Van Driessche), Mike.Sleutel@vub.be (M. Sleutel).

https://doi.org/10.1016/j.jcrysgro.2022.127024
Received 6 October 2022; Received in revised form 26 November 2022; Accepted 28 November 2022
Available online 1 December 2022

that cluster-mediated growth has emerged as a widespread mechanism across a broad range of crystallization environments, such as biomineralization [8], zeolite synthesis [9] and the growth of organic [10] and protein crystals [7,11,12].

Here, we continue our efforts to understand cluster-mediated crystallization in the presence of crystal growth modifiers. As a test case, we studied lysozyme crystallization from highly impure mother liquor solutions. Our interest in this system is twofold: (I) clusters are omnipresent, but can be easily removed through filtration allowing flexibility in the design of experiments, and (II) protein crystals are more amenable to nanoscopic imaging due to slower kinetics and a larger size of the impurity/solute molecules. To resolve the molecular impurity processes and the mesoscopic step dynamics as a function of the crystallization driving force, we employed atomic force microscopic and confocal microscopy. To complement the in situ data we also performed kinetic Monte Carlo simulations to provide molecular level insight of the interaction of impurities with advancing steps. Based on these in situ and in silico results we propose a cluster-mediated stop-and-go model that is relevant to (bio-)crystallization from highly heterogeneous growth environments.

2. Material and methods

2.1. Seed crystals and grow solutions

Tetragonal crystals of model protein hen egg-white lysozyme were grown at 20.0 ± 0.1 °C from a solution containing 70 mg/ml Sigma lysozyme (≤95 % purity), 25 $mg.ml^{-1}$ NaCl and 50 mM sodium acetate (pH 4.5) buffer. After the seed crystals were transferred to an AFM or confocal microscopy observation cell, they were incubated for 5–6 h until the seed crystals were firmly attached to the bottom glass. Before starting the surface characterization, the solution inside the cell was replaced with a solution of desired lysozyme composition and concentration (either two times dialyzed Sigma or Roche (99.0 % purity)).

2.2. In situ observation of crystal growth

Growing faces of crystals were observed at the solution-crystal interface using confocal microscopy. For a number of selected conditions, we also used tapping-mode atomic force microscopy (AFM) to resolve the surface topography. More details about these in situ observation techniques can be found in the supplementary information and previous works [13,14].

In the case of confocal microscopy, the observation cell was placed inside a temperature-controlled stage with Peltier elements, the formation of two-dimensional (2D) islands and spiral hillocks on {1 1 0} faces was observed. The temperature of the observation cell was changed at given time intervals to change the supersaturation of the lysozyme solution inside the cell: the accuracy of the temperature control was ± 0.1 °C. Before and after each experimental run, the protein concentration was determined at 280 nm with $\varepsilon_{280} = 2.64$ $ml.mg^{-1}.cm^{-1}$ using a two-beam spectrophotometer. The solubility was directly determined observing step movement using confocal microscopy [15]. Observations were carried out in the supersaturation range $C\text{-}C_e$ = 0–31 $mg.ml^{-1}$.

2.3. Kinetic Monte Carlo (kMC) simulations

A kinetic Monte Carlo (kMC) [16] computational model was used to study layer-by-layer on pure and comtaminated (0 0 1) surfaces of a typical Kossel crystal. As impurities, 18 units long stoppers were used. A detailed description of the employed methodology can be found in previous works [17,18]. For simplicity, we work on the (0 0 1) Kossel surface with the rate of surface diffusion set to zero and given that we focus on conditions in the kinetic recovery from surface poisoning (i.e. weak driving forces), we only worked in the kinetically-limited regime of crystal growth. As such, depletion effects near the solid–liquid interface are expected to be minimal, and therefore we used an implicit rendition of the fluid that imposes a constant solute concentration.

3. Results and discussion

3.1. Impurities and surface morphology

To contextualize the results presented in this work, the major characteristics of crystal growth in the Sigma-lysozyme system are briefly summarized. From previous mesoscopic confocal microscopy observations, we have learned that impurities adsorb on the surface significantly altering the shape of 2D islands by lowering their aspect ratio ($x \approx y$) and roughen the step edges (Fig. 1). This stands in stark contrast to the smooth steps and morphology ($x \ll y$) of 2D islands obtained when using pure (99.9 %) lysozyme solution [19–21]. When crystals are incubated for long times (>3 days) at low supersaturations ($C\text{-}C_e \leq 15$ $mg.ml^{-1}$), an even more dramatic shift is observed, inverting the long and short axis of 2D islands ($x \gg y$, Fig. 1c). Importantly, the island morphology strongly depends on the solution supersaturation and lens-shaped islands are observed at high supersaturations ($C\text{-}C_e = 30$ $mg.ml^{-1}$), while for the same solution the above-described rounded islands shape is found at lower supersaturation ($C\text{-}C_e = 15$ $mg.ml^{-1}$) (Fig. S1). Due to the limited lateral resolution of the confocal microscopy technique [22] the exact nature of this morphological switch in the Sigma-lysozyme crystallization system remained elusive. For this, we used tapping mode AFM and acquired high-resolution images of the surface reactivity.

In situ AFM observations for relatively pure Roche-lysozyme (~99.0 %) revealed 2D islands with smooth steps and the typical lens-shaped morphology of pure lysozyme solutions, separated by *clean* (i.e. molecularly flat) terraces (Fig. 2a). This picture changes dramatically when the solution of the AFM liquid cell is replaced with a 95 %-lysozyme solution. The steps become heavily serrated (Fig. 2b) and the terraces between steps are densely populated with mesoscopic particles (Fig. 2c). Two types of impurity particles can be distinguished: (I) spherical clusters and (II) linear fibrils16 [16]. The clusters (see Fig. S2) are randomly distributed across the terraces and have diameters ranging from 10 to 200 nm and a height spanning from 5 to 50 nm. These dimensions are not compatible with the dimensions of a single lysozyme molecule (~$2.8 \times 2.8 \times 3.8$ nm^3). On the other hand, the adsorbed fibrils (such as fibrillar oligomeric assemblies of lysozyme, which is known to adopt an amyloid structure under certain conditions [23,24]) display a distinctive interaction with the surface and are mainly aligned with the ⟨0 0 1⟩ direction (Fig. 2c). However, randomly oriented fibrils are also observed (Fig. S2) indicating that a non-specific component to the binding mode might exists as well. Although the length of fibrils varies, the individual fiber dimension on the surface remains constant over time, from which it can be inferred that the fibrils are pre-formed in the solution. The length ranges from 100 nm to a couple of μm. Notwithstanding some variation, the height typically measures 1.5 to 2 nm. Given that such structures, with high affinity for the (1 1 0) face of tetragonal lysozyme crystals, are not observed when using highly purified lysozyme solutions, they must be the result of a molecular aggregation process of, or induced by, the impurity molecules in the liquid bulk [25].

During AFM measurements at low supersaturations, we also collected images with the slow scanning axis disabled. This approach allowed us to follow the relative stability of fibrils on the crystal surface. The kymograph (y-axis represents time) shown in Fig. 2d demonstrates that most fibrils remain attached to the crystal surface for the duration of the imaging, i.e. 226 s.

To confirm that these linear fibrils are responsible for the marked transition of the 2D islands morphology, we used a kMC computational model [6,16–18] to study the shape of 2D islands growing on pure and comtaminated (with linear impurities) (0 0 1) surfaces of a typical Kossel crystal. When a high enough impurity network (corresponding with ~ 5 % of impurities in the bulk) was present on the surface of a Kossel

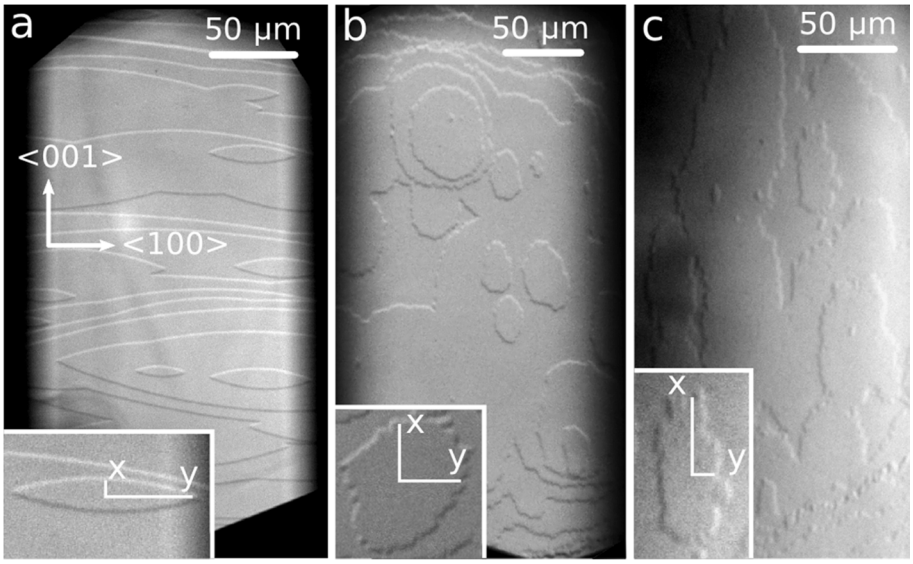

Fig. 1. *In situ* LCM-DIM images of the (1 1 0) face of tetragonal lysozyme crystals growing from pure (a) and contaminated (Sigma) mother liquor solutions (b): the characteristic lens-shaped 2D islands (x≪y) that nucleate under pure conditions transform to more isotropically shaped islands (x≈y) with serrated step edges when exposed to impurities; (c) if this exposure occurs for prolonged times at low supersaturation (C-$C_e \leq 15$ mg.ml^{-1}) a full morphological switch of the aspect ratio is observed (x≫y).

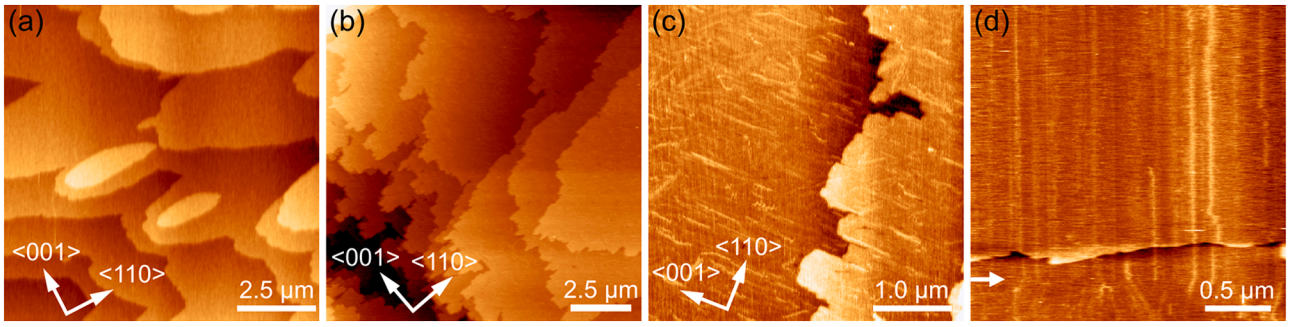

Fig. 2. *In situ* AFM images of the (1 1 0) face of tetragonal lysozyme growing from lysozyme solutions containing impurities: (a) Roche-lysozyme (99.0 % pure), (b-c) Sigma-lysozyme (95.0 % pure), (c) zoom-in of the terraces showing a high density of linear impurities, (d) Time-space plot (starting from the white arrow in upwards direction) of the residence time of linear impurities on the surface (t = 226 s).

crystal, the elongated island configuration (induced by anisotropic interaction energies between solute molecules in the × and y direction being Ey/Ex = 0.54) changed to a more isotropic shape (Fig. 3a,b).

3.2. Linear impurities truncate single- and macro-step advancement

The long residence time of impurities on the surface gives rise to a high-density network of linear impurity chains (cf. Fig. 2c and Fig. S2). This impurity maze severely limits the step advancement, in an orientation dependent manner, resulting in a highly non-linear v_{step} versus C-C_e dependence. This stands in sharp contrast to the near-linear dependence that is obtained when a pure (~99.9 %) lysozyme solution is used (Fig. 4). A dead zone was observed for C-$C_e \approx 0$–10 mg.ml^{-1}, and minimal step movement was detected for the supersaturation range C-C_e

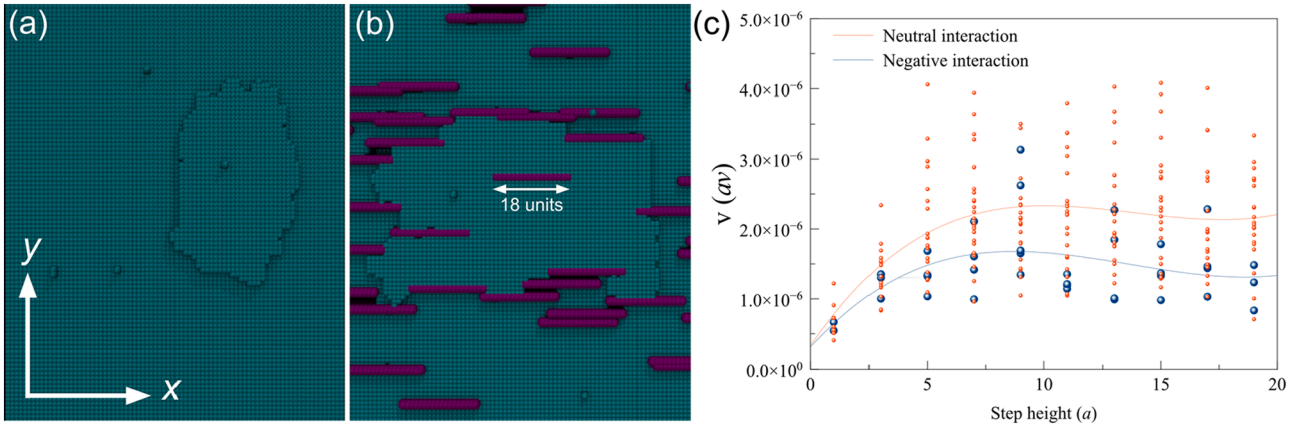

Fig. 3. Snapshots from kMC simulations, showing 2D islands formed on (a) pure and (b) contaminated Kossel surface. (c) Step velocity v as a function of macrostep height a for a neutral and negative interaction of the impurities with the overgrowing layer.

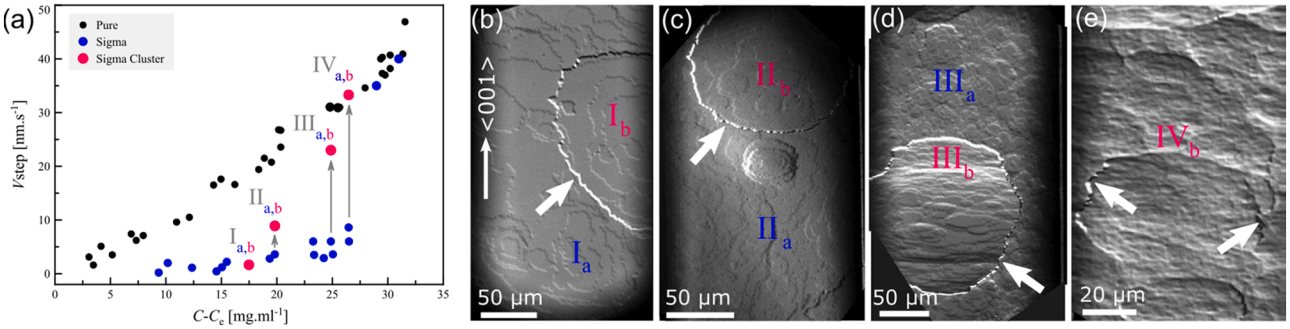

Fig. 4. Supersaturation dependence of impurity cleansing by 3D islands: (a) Dependence of v_{step} on the absolute supersaturation C-C_e for pure (black) and impure (blue) conditions, measured along the ⟨1 1 0⟩ direction. re-acceleration of the steps towards the rate measured for pure conditions is observed when terraces enclosed by looped macrosteps are formed as a result of the merger between mesoscopic clusters and the crystal surface (red). The experimental conditions between Sigma and Sigma Cluster are otherwise identical. *In situ* LCM-DIM snapshots of cluster mediated self-purification on the (1 1 0) face of tetragonal lysozyme crystals at different supersaturations: (b) C-C_e = 17.5 mg.ml^{-1}, (c) C-C_e = 20 mg.ml^{-1} (d) C-C_e = 25 mg.ml^{-1} (e) C-C_e = 27 mg.ml^{-1}. White arrows indicate the position of macrosteps. Roman numbers signalize the area of measurements corresponding with the step velocities shown in (a). (For interpretation of the references to colour in this figure legend, the reader is referred to the web version of this article.)

≈ 10–25 mg.ml^{-1}. At C-C_e ≥ 25 mg.ml^{-1}, a steep increase in step velocity, associated with a drastic change in step morphology (see Fig. S1), is observed for crystals growing from a Sigma-lysozyme solution. None of the conventional kinetic impurity models [1] (e.g. Cabrera-Vermilyea, Bliznakov, Frank) can capture this supersaturation dependence and predict the system switching between two different kinetic modes [26]. Also noteworthy is the fact that single and macro-steps move at a similar velocity (within the margin of the experimental error) through the impurity network. This observation contradicts with recent experimental and simulations results, which have shown that macrosteps can advance at low supersaturation and high impurity density while elementary steps remain pinned [5,6]. This discrepancy could be, at first sight, due to effective blocking of macrosteps by linear impurities.

To obtain a mechanistic understanding of these experimental observations we monitored in silico the growth of single– and macrosteps in the presence of linear impurities using kMC simulations [6,16–18]. We populated the surface with a fixed density of linear impurity atoms and monitored the kinetics of growth for a broad range of step heights N. We obtained that the step velocity increases as a function of macrostep height, which plateaus after a certain number of layers (Fig. 3c). This observation is in line with our previous work on point impurities [6], where we have shown that breaching of the impurity-dense regions occurs in two-steps, first a monolayer is pushed through the impurity spacing and is followed by nucleation of a 3D cluster on the intersection between the vicinal surface and the facet defined by the macrostep (Fig. S3). However, in the current simulations we observed a much weaker dependency of step velocity on the step height. Hence, the breaching of the impurity fence by macrosteps appears to be less effective in the presence of linear impurities.

Up to now, we only considered neutral impurities, i.e. all interaction energies were set to zero apart from the downward interaction used to fix the impurities onto the surface. When we consider mildly repulsive solute-impurity interactions vertically upward (between the impurity molecules and the overgrowing layer), than the difference in step velocity between single and multi-layered steps is further dampened. Hence, vertical repulsive interactions cancel out the advantage multi-step might have to overrun the impurities fence observed in previous works [5,6,18].

3.3. Impurity cleansing by cluster mediated multi-layered islands

But, an alternative escape route from this dead zone becomes available when mesoscopic lysozyme clusters [7,27,28] land on the impurity poisoned surface and closed looped macrostep are formed. The nucleation or attachment of 3D particles on a crystal surface is not uncommon for growth from solution and has been observed for both macromolecules e.g. [7,10,11,12] and small molecules e.g. [29,30].

In our experiments we observed that when a mesoscopic cluster impacts on the surface, and a 3D island is formed, the crystal surface managed to break through the impurity fence (a time sequence of the fast recovery of a crystal surface mediated by a 3D island is shown in Fig. 5). The newly formed (1 1 0) surface on top of such a 3D island has a significantly lower impurity concentration compared to the underlying poisoned surface. This is directly evidenced by the difference in 2D islands morphology and a significant difference in step velocity (e.g. Fig. 4d). But, this did not occur at all supersaturations were we observed the nucleation/attachment of a 3D cluster. To help us with the interpretation of this particular crystal growth event, we take advance of the fact that multiple growth states can be observed on a single crystal surface. Fig. 4b-e shows a crystal surface at different supersaturations. After close inspection it becomes apparent that depending on the supersaturation level at which the 3D island appeared the step velocities on its top layer will be closer or further away from the pure case. Starting from a threshold supersaturation (C-C_e ≈ 20 mg.ml^{-1}) a significant increase in step velocity on top of a 3D island with respect to the underlying surrounding surface is reached. With increasing supersaturation, C-C_e ≈ 25 mg.ml^{-1}, the step velocity on top of a 3D island further increases and is associated with a noticeable change in the morphology of 2D islands (Fig. 4d). At a slightly higher supersaturation the system is pushing towards near pure velocities. Hence, the effectiveness of this escape route from the dead zone is directly related to the supersaturation at which a cluster forms on / merges with the crystal surface.

Traditional impurity recovery models consider only elementary steps and at first sight are not applicable to describe the surface reactivity of this system. Notwithstanding, close inspection of the images shown in Figs. 6 and 7 reveals that macrosteps are not responsible for cleansing of the surface, as observed for KDP crystals [5,31], but rather the dynamics of single steps on top of 3D islands (i.e. multilayer 2D islands). The behaviour of two multilayer steps (MS), one advancing on top of the other (MS1 and MS2, Fig. 6a), exemplifies this principle. While MS1 is moving in contact with the original impurity poisoned surface, and thus experiencing the dense network of linear fibers, its velocity is identical (within experimental error) to that of monolayer steps on that surface, i.e. v_{MS1}≈v_0 (Fig. 6b). In contrast, the step dynamics of MS2 are comparable to those of the monolayer islands growing on top of the MS1, at a velocity much higher than v_0, i.e. v_{MS2}≈v_1≫, v_{MS1}≈v_0. Thus, MS2 should catch up with MS1, which is nicely illustrated in the time sequence shown in Fig. 6. This provides direct evidence that on top of a multi-layered island a surface is created relatively devoid of impurities, and

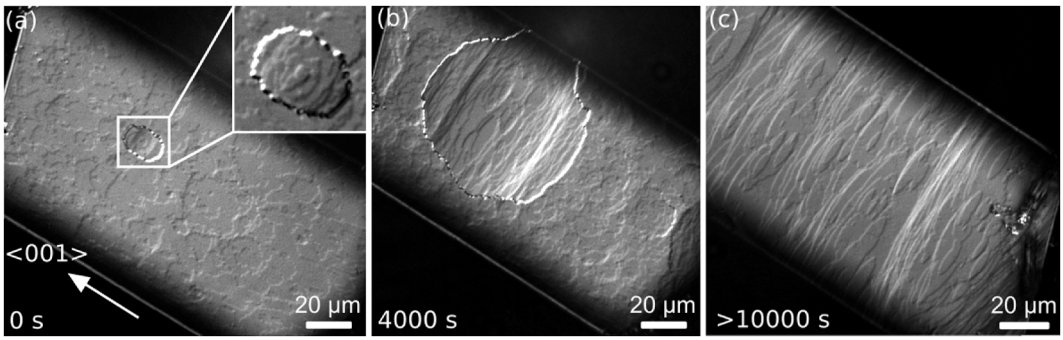

Fig. 5. Time sequence of a cluster mediated surface cleansing event: this start when a cluster merges with the crystalline surface and induces the formation of a 3D island [1] (a), which continuously expands covering the impurity-poisoned surface (b), and eventually leaves a cleansed surface behind (c).

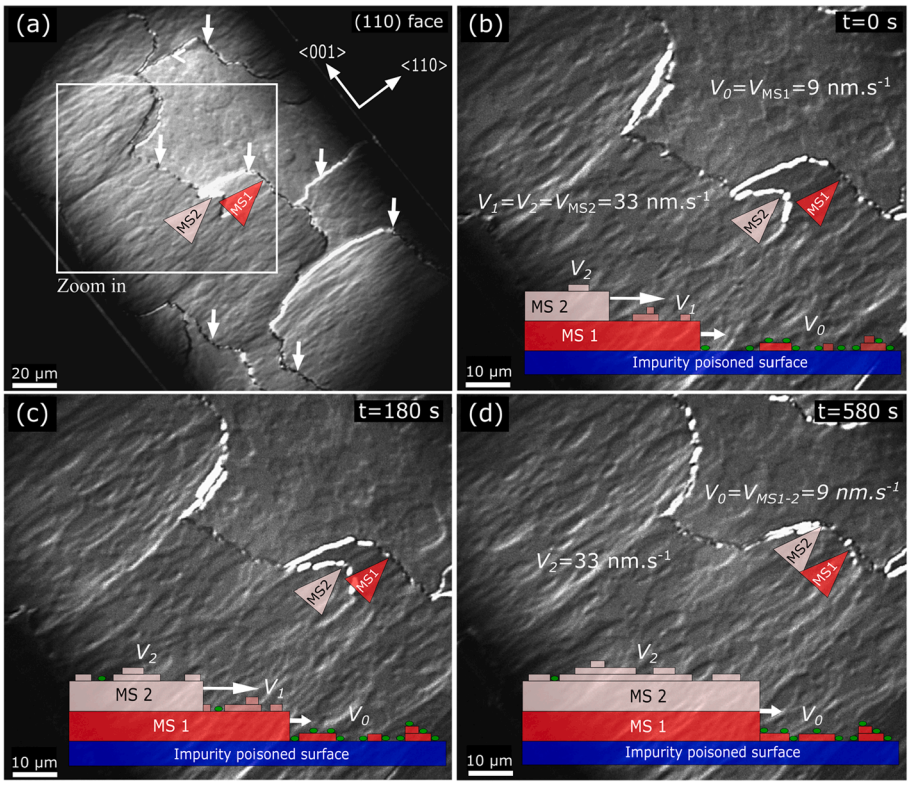

Fig. 6. Cluster-mediated surface purification: (a) mesoscopic laser confocal microscopy images of the (1 1 0) face of a tetragonal lysozyme crystal exposed to Sigma mother liquor solutions. The white arrows indicate macrostep edges that are the result of the merger of liquid-like protein clusters with the crystal surface; (b)-(d) successive zoom-ins of the area delimited by the white square in (a): the bottom macrostep (red arrowhead) advances at a far lower rate (9 nm.s^{-1}) than the macrostep progressing on its terrace (33 nm.s^{-1}, pink arrowhead). (For interpretation of the references to colour in this figure legend, the reader is referred to the web version of this article.)

as a consequence the step velocity of newly formed mono-and multilayer steps on top of a 3D island will have a significantly higher step velocity than those formed on the impurity poisoned surface, i.e. $v_0 \ll v_1$ (Figs. 4 and 7). Due to the much higher step velocity, the terrace exposure time is significantly reduced and the newly formed surface is "protected" from further impurity poising. This is also reflected in the shape of the 2D islands, which will belong elongated (Fig. 7a,b).

When such a surface, depleted of impurities, is created at a high enough supersaturation, the shorter terrace exposure time on this surface will not allow for impurities to adsorb and thus create a new layer with even less impurities leading to an increase in step velocity overtime (Fig. 7c). The step velocity on top of the 3D island will continue to increase until a new equilibrium between terrace exposure and impurity adsorption is established, while the step velocity of the original surface will remain constant (Fig. 7c). Hence, depending on the supersaturation at which the 3D cluster appeared the final step velocity will be further or closer to the step velocity of a pure solution (Fig. 7d and Fig. 4).

Concluding, our in situ observations reveal that the formation of 3D islands can lead to less contaminated crystal surface and pave the way for the system to escape from the growth dead zone. The mechanism of this escape route can be summarized as follows: (1) a mesoscopic protein cluster merges with a impurity poisoned crystal surface creating a 3D island with a "fresh" top layer containing a reduced amount of impurities (most likely originating from the mesoscopic cluster), (2) depending on the supersaturation level at which a 3D island is formed the new surface layer will have a corresponding 2D nucleation rate and step velocity establishing a terrace exposure time, which, in turn, will fix the maximum amount of impurities adsorbed on the surface (being this a function of the characteristic impurity adsorption time- terrace exposure time ratio). Over time, a new steady state will be established on top of such a 3D island. The multi-layered step enclosing the 3D island will slowly sweep across the impurity-poisoned surface, until the crystal edges are reached (Fig. 5) establishing a new surface state for the entire crystal face.

4. Implications

The concept of particle-mediated nucleation was introduced during

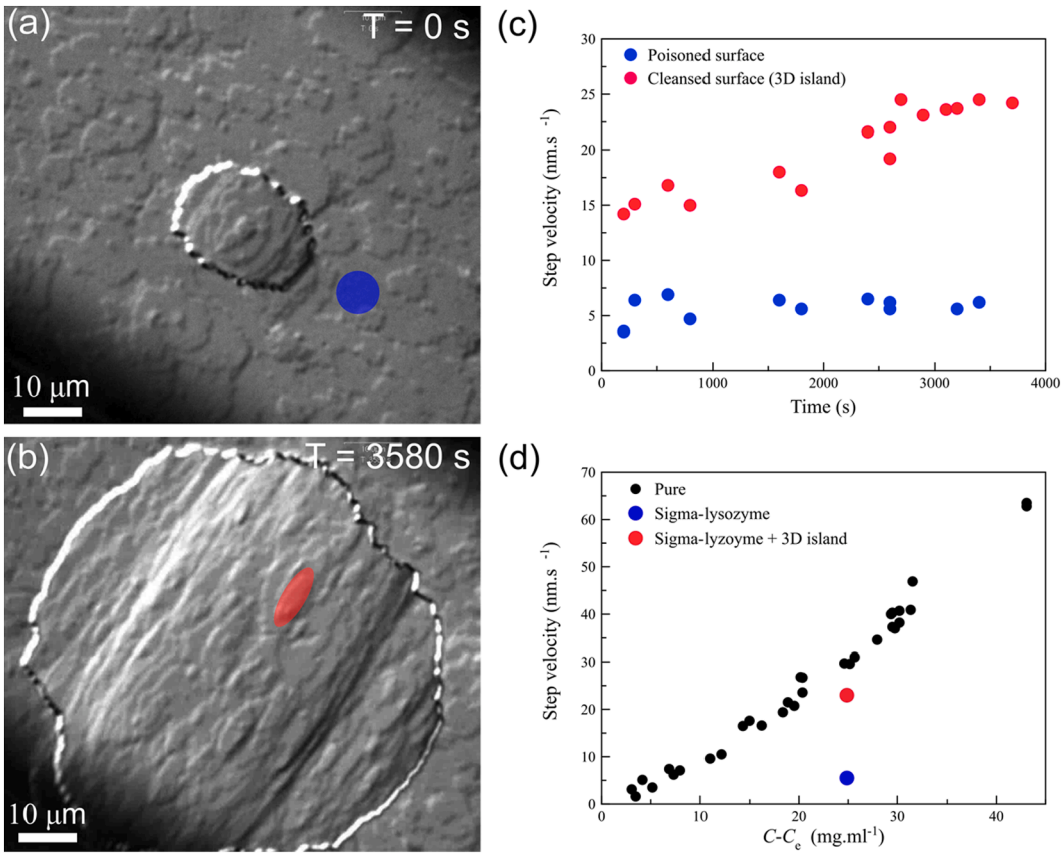

Fig. 7. Evolution of 2D islands on top of a 3D island and a poisoned surface of a tetragonal crystal growing from a Sigma-lysozyme solution: (a-b) Characteristic 2D island morphology for the cleansed and poisoned surfaces, schematically represented by red and blue ellipsoids; (c) Time dependence of the step velocity, on both surfaces, after the formation of a 3D island; (d) Steady state step velocity of both surface locations compared to step velocity measured for pure-lysozyme. (For interpretation of the references to colour in this figure legend, the reader is referred to the web version of this article.)

this last decade, and is now widely accepted as an important mineralization route [32,33]. Recent studies have also shown that, under certain conditions, clustered species can play an key role during the crystal growth stage of both organic and inorganic systems [7,10,11,12,29,30]. Particularly, in biomineralization evidence has been gathered showing how spicule growth does not proceed by incorporation of single atoms, as in classical crystal growth from solution, but instead transient clustered phases [8,34] appear to be the main building units. On the other hand, in many natural mineralization processes, chain-like, i.e. linear, impurities play a pivotal role including: (I) growth modulation of calcite by alginate [35], (II) inhibition of calcium oxalate monohydrate precipitation by linear aspartic acid enantiomers [36], or (III) control of apatite growth by phosphorylated proteins[37]. The insights presented here allow to merge both aspects – clusters and linear impurities – into a single crystal growth model, which is readily transferable to mineralization taking place in highly heterogeneously environments, e.g. rich in peptide/protein molecules. Thus, based on our in situ and in silico observations, we propose that cluster-mediated crystal growth combined with linear impurities can lead to stop-and-go crystallization, a mechanism that can could be key to understand (bio-)crystal formation in biological influenced and/or controlled crystallization.

CRediT authorship contribution statement

A.E.S. Van Driessche: Conceptualization, Methodology, Writing – review & editing. **J. Lutsko:** Software, Writing – review & editing. **D. Maes:** Writing – review & editing. **M. Sleutel:** Conceptualization, Methodology, Writing – review & editing.

Declaration of Competing Interest

The authors declare that they have no known competing financial interests or personal relationships that could have appeared to influence the work reported in this paper.

Data availability

Data will be made available on request.

Acknowledgements

This work was partially supported by the European Space Agency under Contract No. ESA AO-2004-070, FWO grant 1523115 N (Belgium) and scholarship BES·2003·2191 (AVD, Ministerio de Ciencia y Tecnologia, Spain).

Appendix A. Supplementary material

Supplementary data to this article can be found online at https://doi.org/10.1016/j.jcrysgro.2022.127024.

References

[1] A.A. Chernov, Modern Crystallography III, Crystal Growth, Springer Series on Solid State Science, vol. 36, published by Springer, Berlin, Heidelberg, New York, Tokyo, Part I, 1984.
[2] K. Sangwal, Additives and Crystallization Processes: From Fundamentals to Applications, John Wiley & Sons, Chichester, England, 2007.
[3] S.Y. Potapenko, J. Cryst. Growth 133 (1993) 141–146.
[4] K. Sangwal, Prog. Cryst. Growth Charact. Mater. 32 (1996) 3–43.

[5] T.A. Land, T.L. Martin, S. Potapenko, G.T. Palmore, J.J. DeYoreo, Nature 399 (1999) 442–445.
[6] Lutsko, J.; Van Driessche, A.E.S.; Duran-Olivencia; Maes, D.; Sleutel, M. Phys. Rev. Lett. 2106, 116, 15501.
[7] M. Sleutel, A.E.S. Van Driessche, Proc. Nat. Acad. Sci. USA 111 (2014) 546–553.
[8] P.U.P.A. Gilbert, S.M. Porter, C.-Y. Sun, S. Xiao, B.M. Gibson, N. Shenkar, A. H. Knoll, Proc. Natl. Acad. Sci. U.S.A. 116 (2019) 17659–17665.
[9] Kumar, M.; Luo, H.; Román-Leshkov, Y.; Rimer, J.D. J. Am. Chem. Soc. 137 (40), 13007–13017.
[10] Y. Jiang, M. Kellermeier, D. Gebauer, Z. Lu, R. Rosenberg, A. Moise, M. Przybylski, H. Colfen, et al., Nat. Commun. 8 (2017) 15933.
[11] O. Gliko, N. Neumaier, W. Pan, I. Haase, M. Fischer, A. Bacher, S. Weinkauf, P. G. Vekilov, J. Am. Chem. Soc. 127 (2005) 3433–3438.
[12] A.E.S. Van Driessche, N. Van Gerven, R.R.M. Joosten, et al., Nat. Commun. 12 (2012) 3902.
[13] A.E.S. Van Driessche, F. Otalora, G. Sazaki, M. Sleutel, K. Tsukamoto, J.A. Gavira, Cryst. Growth Des. 8 (2008) 4316–4323.
[14] A.E.S. Van Driessche, Sleutel. M. Cryst. Res. Tech. 48 (2013) 919–941.
[15] A.E.S. Van Driessche, J.A. Gavira, L.D. Patiño Lopez, F. Otalora, J. Cryst. Growth 311 (2009) 3479–3484.
[16] J. Lutsko, N. González-Segredo, A. Durán-Olivencia, D. Maes, A.E.S. Van Driessche, M. Sleutel, Cryst. Growth Des. 14 (2014) 6129–6134.
[17] M. Sleutel, J. Lutsko, D. Maes, A.E.S. Van Driessche, Phys. Rev. Lett. 114 (2015), 245501.
[18] M. Sleutel, J. Lutsko, A.E.S. Van Driessche, Cryst. Growth Des. 18 (2018) 171.
[19] P. Dold, E. Ono, K. Tsukamoto, G. Sazaki, J. Cryst. Growth 293 (2006) 102–109.
[20] A.E.S. Van Driessche, In Situ Observation of Protein Crystal Growth by Advanced Optical Techniques, Granada, 2007.
[21] M. Sleutel, G. Sazaki, A.E.S. Van Driessche, Cryst. Growth Des. 12 (2012) 2367–2374.
[22] A.E.S. Van Driessche, F. Otalora, G. Sazaki, M. Sleutel, K. Tsukamoto, J.A. Gavira, Cryst. Growth Des. 8 (2008) 4316–4323.
[23] D.R. Booth, M. Sunde, V. Bellotti, C.V. Robinson, W.L. Hutchinson, P.E. Fraser, P. N. Hawkins, C.M. Dobson, S.E. Radford, C.C. Blake, M.B. Pepys, Nature 385 (1997) 787–793.
[24] Y. Zou, W. Hao, H. Li, Y. Gao, Y. Sun, G. Ma, J. Phys. Chem. B 118 (2014) 9834–9843.
[25] L.A. Morozova-Roche, J. Zurdo, A. Spencer, W. Noppe, V. Receveur, D.B. Archer, M. Joniau, C.M. Dobson, J Struct Biol 130 (2000) 339–351.
[26] M. Sleutel, A.E.S. Van Driessche, Cryst. Growth Des. 13 (2013) 688–695.
[27] Y. Georgalis, P. Umbach, W. Saenger, B. Ihmels, D.M. Soumpasis, Ordering of Fractal Clusters in Crystallizing Lysozyme Solutions, J. Am. Chem. Soc. 121 (8) (1999) 1627–1635.
[28] W. Pan, P.G. Vekilov, V. Lubchenko, Origin of Anomalous Mesoscopic Phases in Protein Solutions, J. Phys. Chem. B 114 (22) (2010) 7620–7630.
[29] A.E.S. Van Driessche, J.M. García-Ruiz, J.M. Delgado-Lopez, G. Sazaki, Cryst. Growth Des. 10 (2010) 3909–3916.
[30] A.I. Lupulescu, J.D. Rimer, Science 344 (2014) 729–733.
[31] T.N. Thomas, T.A. Land, W.H. Casey, J.J. De Yoreo, Phys. Rev. Lett. 92 (2004), 216103.
[32] J.J. De Yoreo, P.U.P.A. Gilbert, N.A.J.M. Sommerdijk, R.L. Penn, S. Whitelam, D. Joester, H. Zhang, J.D. Rimer, A. Navrotsky, J.F. Banfield, et al., Science 349 (2015) aaa6760.
[33] A.E.S. Van Driessche, M. Kellermeier, L.G. Benning, D. Gebauer (Eds.), New Perspectives on Mineral Nucleation and Growth, Springer International Publishing, Cham, 2017.
[34] E. Beniash, J. Aizenberg, L. Addadi, S. Weiner, Proc. R. Soc. B. Lond. Biol. Sci. 264 (1997) 461–465.
[35] L.Z. Lakshtanov, N. Bovet, S.L.S. Stipp, Geochim. Cosmochim. A. 75 (2011) 3945–3955.
[36] K.R. Cho, E.A. Salter, J.J. DeYoreo, A. Wierzbicki, S. Elhadj, Y. Huang, R.S. Qiu, CrstEngComm 15 (2013) 54–64.
[37] A. George, A. Veis, Chem. Rev. 108 (2008) 4670–4693.